Table of contents

Figure S1. Schematic illustration of the laser trigger and the PMT detection components.

The PMT (photomultiplier tube) used in this system can achieve single photon counting, providing strong support for the high sensitivity of the entire system. The weak 680nm emitted light hits the PMT cathode light window in the form of photons and excites photoelectrons. The quantum efficiency of the light window exceeds 25%. A high voltage of more than 1000V is applied between the anode and cathode of the PMT, and the voltage is divided between each electrode according to a specific ratio. The cathode photoelectrons bombard secondary electrons at each electrode under high voltage. A gain of more than 2*106 can be achieved from the cathode to the anode, and a current pulse that can be identified is generated at the anode.

The current pulse signal is converted into a voltage pulse signal that can be detected by micro-processing through amplification and IV changes corresponding to single photons, and ultimately, the counting of single photons is achieved, ensuring the system's high sensitivity.

In the detection optical path part, the 6nm laser has a built-in filter with a bandwidth of 10nm to achieve a single and controllable laser wavelength. Combined with the value acquisition principle, the laser is turned on intermittently, and there is no need to prepare a separate heat dissipation module; in the receiving part, in order to adapt to the size of the instrument, a miniature low-noise photomultiplier tube is used, with a dark current of ≤20nA, further improving the measurement sensitivity.

As shown in Figure S2, the laser and the PMT are vertically aligned, enabling simultaneous laser excitation and optical detection.

Quality assurance of temperature control systems: The incubation module is utilized for incubating reagents in the reagent tray and maintaining a stable reaction environment at 37± 0.5 °C. This module comprises a stainless-steel heat conduction plate attached to two upper and lower PI film heating sheets. A miniature Negative Temperature Coefficient (NTC) thermistor with thermal conductive silicone grease is embedded in each thermally conductive plate to achieve precise control of the ambient temperature. Furthermore, the instrument's built-in ambient temperature monitoring sensor allows the heating control method to be adjusted based on the current ambient temperature, thereby reducing the temperature fluctuations in the reaction zone.

As shown in Figure 1B, the incubation chamber of the instrument contains two heating plates. After the reagent plate enters the incubation chamber, it is wrapped by the two heating plates to achieve uniform incubation. An NTC temperature sensor is embedded in the upper and lower heating plates and the back cover of the machine. After obtaining the ambient temperature, the actual temperature of the incubation chamber is indirectly controlled by adjusting the parameters of the proportional-integral-derivative (PID) temperature controller unit and the target temperature of the upper and lower heating sheets. The basic formula of the PID control unit is:

$$\mu(t) = K_p e(t) + K_i \int_0^t e(\tau)d\tau + K_d \frac{de(t)}{dt} \quad (1)$$

$\mu(t)$ is the control output.

e(t) is the error, which is the difference between the setpoint and the process variable.

K_p is the proportional gain.

K_i is the integral gain.

K_d is the derivative gain.

To establish the actual relationship between the temperature of the detection cavity in the panel, the temperature of the upper and lower heating sheets, and the ambient temperature, a Bluetooth-transmitted temperature sensor tooling is designed. The shape of the tool body is the same as that of the reagent tray. A temperature sensor chip is embedded in the radius direction of the detection chamber. When monitoring the temperature, the tool will be locked on the motor tray to simulate the operation of the actual cartridge. The temperature data obtained through this matter is used to establish a relationship with the temperature of the heating plate.

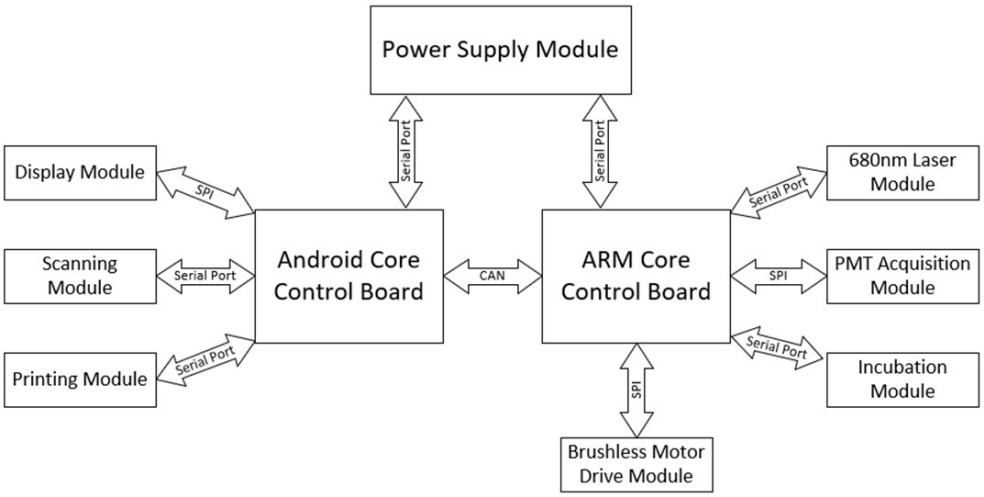

Figure S2. Hardware framework of the multiplexed centrifugal microfluidic LICA system

The hardware framework mainly includes two core modules, one is the Android control core board for interacting with users and issuing commands, and the other is the ARM core control board for controlling all the underlying drivers of the instrument: the user application layer includes the display control module, the code scanning module, the printing module, etc.; the underlying driver layer includes the 680nm laser emission module, the PMT signal receiving and processing module, the incubation module, and the brushless motor control module.

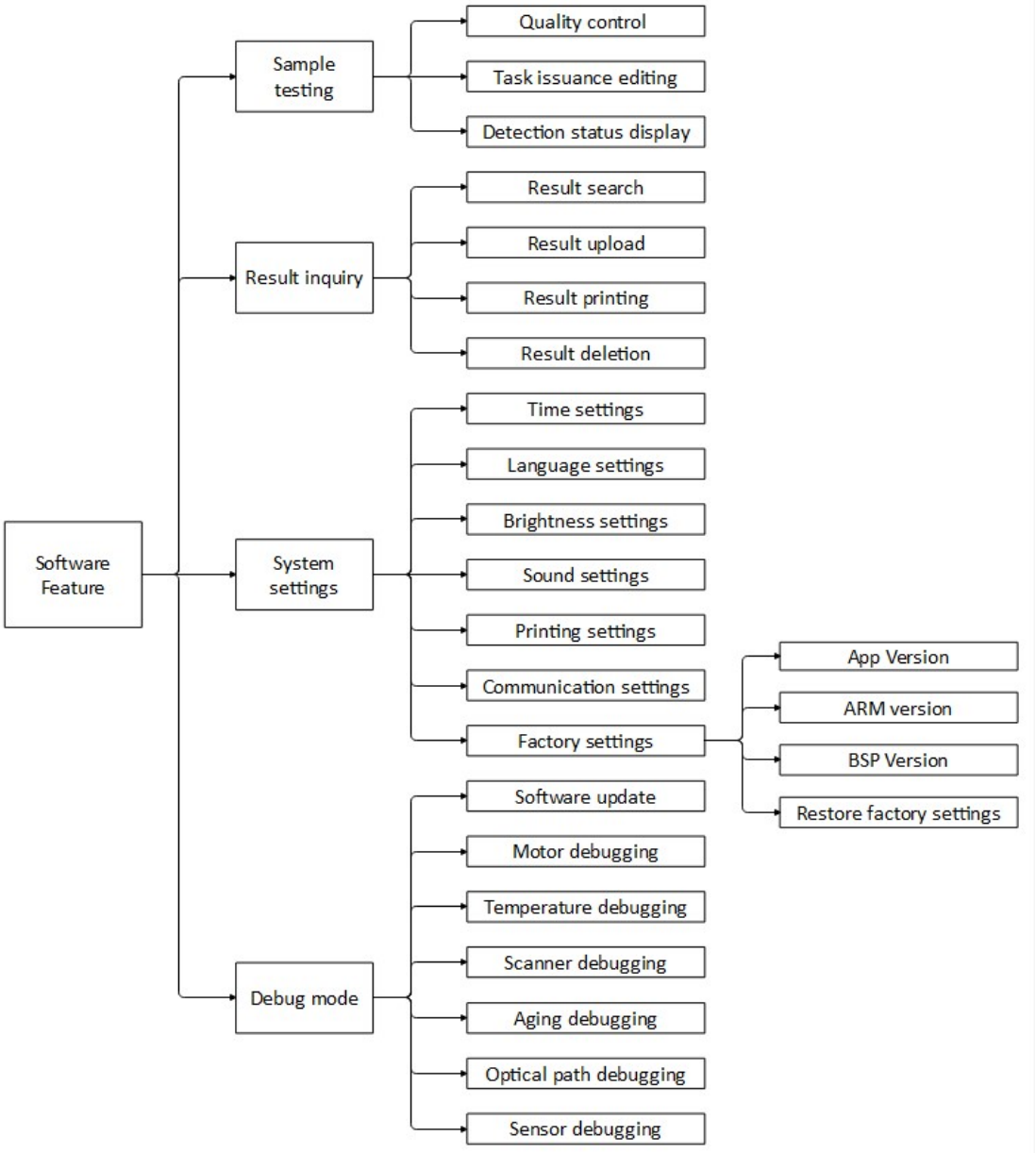

Figure S3. Software framework of the multiplexed centrifugal microfluidic LICA system

The software framework includes a sample analysis module, a results query module, a system settings module, and a debugging module. The sample analysis module contains quality control functions, task dispatch editing, and status monitoring during the detection process. The results query module includes querying, uploading, printing, and deleting results. The system settings module includes basic functions such as brightness adjustment, in addition to supporting queries for firmware versions. The debugging module includes firmware upgrades, motor, whole machine aging, light path, and in addition, it supports queries for some sensor states inside the whole machine.

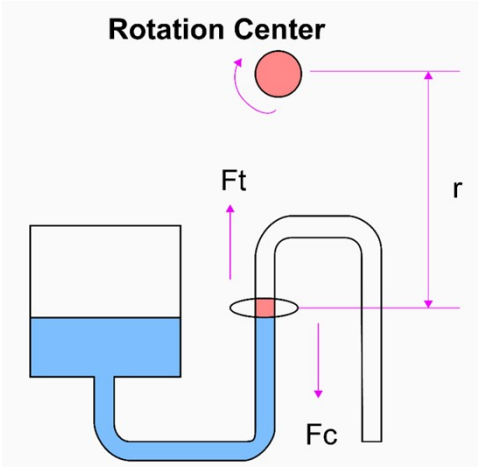

Figure S4. Schematic illustration of the pseudo-forces acting in centrifugal microfluidics.

As shown in Figure S1, the quantification and transfer of the sample and diluent are completed through a separate quantification chamber and capillary tube in the kit. In principle, for a disc driven by centrifugal force, the quantification and transfer of liquid in the disc are determined by the relative magnitudes of centrifugal force and capillary force.

The centrifugal force can be expressed as:

$$Fc=m\cdot r\cdot\omega 2 \tag{2}$$

Where r is the distance between the object and the axis of rotation

ω is the angular velocity of the object

Capillary force can be expressed as:

$$Ft=2\pi r\gamma\cos(\theta) \tag{3}$$

F is the size of capillary force,

r is the radius of the capillary,

γ is the surface tension of the liquid,

θ is the contact angle between liquid and solid

It can be known from the above formula that when the structural size and material of the reagent disk are selected, by increasing the rotation speed of the reagent disk, it can be ensured that the liquid in the pink part cannot cross the highest point of the U-shaped tube and form a siphon. This step can complete the quantitative operation.

If the rotation speed of the reagent disk is reduced, the centrifugal force will gradually decrease until it is lower than the inherent capillary force of the reagent disk. The U-shaped tube will be jumped over, and a siphon effect will be formed. Through this step, the transfer operation can be completed.

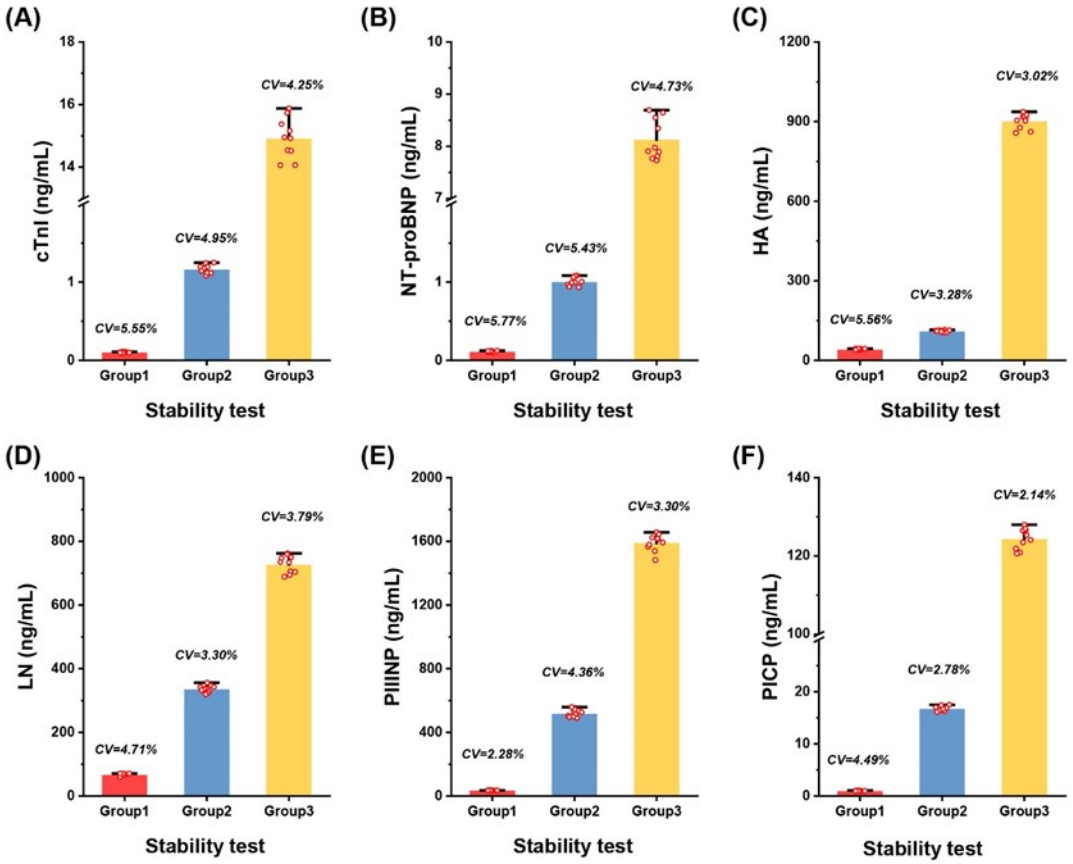

Figure S5. Stability test results of the six biomarkers using three different levels (low, medium and high concentrations) of quality control materials.

Stability test of the assay is conducted by measuring three levels (low, medium, high) of reference materials of each biomarker 10 times and analyzing the coefficient of variance (CV). As shown in Figure S4, the CV of each test series is generally satisfactory, indicating that the repeatability of the LICA system is good and there is no systematic error affecting the accuracy and repeatability of the test results.

Table 1. Test results (ng/mL) of six biomarkers in LGE negative and positive patients.

	Negative (N=100)	**Positive (N=90)**
HA	47.46 ± 20.08	88.99 ± 38.79
LN	40.11 ± 19.26	71.87 ± 14.85
NT-proBNP	0.6516 ±0. 3317	1079.0 ± 202.9
cTnI	0.0126 ± 0.0105	0.0270 ± 0.0142
PIINP	358.5 ± 174.2	677.3 ± 151.9
PICP	74.85 ± 34.14	110.8 ± 16.56

Table 2. Diagnostic efficacy of six markers detected by the LICA system

	AUC	95% CI	SE	SP	Cut-off value (ng/mL)
HA	0.772	0.704-0.840	65.6%	84.0%	66.115
LN	0.752	0.684-0.820	66.7%	72.0%	56.040
NT-proBNP	0.670	0.593-0.747	76.7%	56.0%	0.655
cTnI	0.548	0.466-0.630	97.8%	11.0%	0.003
PIIINP	0.833	0.778-0.889	84.4%	66.0%	479.875
PICP	0.713	0.638-0.788	44.4%	98.0%	115.410

Table 3. LoD comparison between the LICA system and Abbott system

Biomarkers	LoD	
	LICA system (ng/mL)	**Abbott system (ng/mL)**
cTnI	0.0018	0.0012
NT-proBNP	0.0127	0.0079
HA	3.52	5.12
LN	6.88	5.23
PIIINP	4.68	2.74
PICP	0.072	0.071